Journal of the Ceramic Society of Japan 128 [5] 260-266 2020
DOI http://doi.org/10.2109/jcersj2.20037

JCS-Japan

FULL PAPER

Synthesis and color development mechanism of $Li_2CoTi_3O_8$ cyan pigments: effect of synthetic temperature

Saho KIMURA[1], Yuki KANEKO[1], Kazuhiro MARUMOTO[1,2] and Yoshikazu SUZUKI[1,2,†]

[1] Graduate School of Pure and Applied Sciences, University of Tsukuba, 1–1–1 Tennodai, Tsukuba, Ibaraki 305–8573, Japan
[2] Faculty of Pure and Applied Sciences, University of Tsukuba, 1–1–1 Tennodai, Tsukuba, Ibaraki 305–8573, Japan

$Li_2CoTi_3O_8$ has a spinel-type crystal structure, and it can be simply synthesized by a solid-state method using Li_2CO_3, CoO and TiO_2. $Li_2CoTi_3O_8$ is currently used as a cyan-colored pigment, and it is highly safe as is actually utilized for cosmetics. In this paper, we have studied the color development mechanism of $Li_2CoTi_3O_8$ with changing the synthetic temperatures, using X-ray diffraction (XRD), CIE-$L^*a^*b^*$ color coordinates, hue angle h, UV–Vis spectroscopy, X-ray photoelectron spectroscopy (XPS) and electron spin resonance (ESR). $Li_2CoTi_3O_8$ formation was partially confirmed even at 500 °C, and single-phase $Li_2CoTi_3O_8$ was obtained at 950–1200 °C. All the samples synthesized at 750–1200 °C located in the cyan color zone ($h \sim 195$–$235°$). The color change with synthetic temperatures, from whitish to deep cyan, was well explained by the visible light absorptions of Co^{2+} ions with different coordinations.

Key-words : $Li_2CoTi_3O_8$, Spinel, Inorganic pigment, Solid state synthesis, Cyanic blue

[Received February 10, 2020; Accepted March 8, 2020]

1. Introduction

Blue is one of the most common colors in nature, but creating a blue color has been historically difficult. Up to now, a variety of inorganic blue pigments have been synthesized, such as cobalt blue ($CoAl_2O_4$),[1)–4)] lanthanum-strontium copper silicates ($Sr_{1-x}La_xCu_{1-y}Li_ySi_4O_{10}$),[5)] hibonite-based compounds, $AAl_{12-x}M_xO_{19}$ (A = Ca, Sr, or rare earths, M = Ni etc.),[6)] turquoise blue ($Li_{1.33}Ti_{1.66}O_4$),[7)] calcium europium scandium silicate garnet [$(Ca_{1-x}Eu_x)_3Sc_2Si_3O_{12+\delta}$],[8)] $YIn_{1-x}Mn_xO_3$ solid solution[9)] and lithium cobalt titanate ($Li_2CoTi_3O_8$).[10)–14)]

Among the inorganic blue pigments, we have recently focused on $Li_2CoTi_3O_8$.[14)] $Li_2CoTi_3O_8$ has a spinel-type crystal structure with a space group of $P4_332$, a = 8.3766(12) Å (**Fig. 1**).[15)–17)] $Li_2CoTi_3O_8$ has also been studied as an anode material for lithium ion batteries due to its high specific lithium storage capacity and high electronic conductivity.[17)–19)] $Li_2CoTi_3O_8$ can be simply synthesized by a solid state method using Li_2CO_3, CoO and TiO_2 powders.

$Li_2CoTi_3O_8$ is highly safe and is used as a cyanic blue pigment. In particular, it is currently used for cosmetics.[10)–14)] $Li_2CoTi_3O_8$ is excellent in acid and alkali resistance, light resistance and heat resistance. In our previous report,[14)] we have demonstrated that the colors of CoO-lean compositions and stoichiometric $Li_2CoTi_3O_8$ are substantially same (cyanic blue). Quantitative color measurement revealed that 10% reduction of CoO from stoichiometric $Li_2CoTi_3O_8$ is possible without much affecting the human eye feeling. This result encourages further reduction of Co resources for the production of $Li_2CoTi_3O_8$ pigment. In addition, we have also demonstrated that green color pigments can be synthesized just by increasing the CoO compositions.[14)] The green colors appeared for the CoO-rich compositions, and the dichroism of the $Li_2CoTi_3O_8$ pigment was attributable to the valence change of Co ions from divalent (cyanic) to trivalent (greenish).

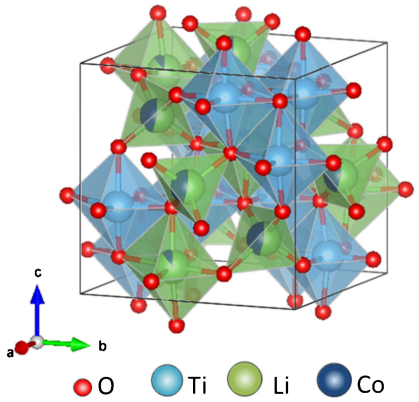

Fig. 1. Crystal structure of $Li_2CoTi_3O_8$ drawn with a reported data by Kawai et al.[15)] In the spinel structure, Co^{2+} ions exist as both tetrahedral and octahedral coordinations. Reproduced with permission from [14] with the license No. 4783410176454. Copyright 2019 Elsevier.

† Corresponding author: Y. Suzuki; E-mail: suzuki@ims.tsukuba.ac.jp

Besides the cobalt composition, synthetic temperature will also affect the color tone of $Li_2CoTi_3O_8$ pigment. Costa da Câmara et al.[12] reported the effect of synthetic temperature on color tone of sol–gel derived $Li_2CoTi_3O_8$. They reported that the pigment presented green color at the synthetic temperature of 400–500 °C and blue color at that of 600–1000 °C. Such a dichroism of the $Li_2CoTi_3O_8$ pigment is attributable to the valence change of Co ions from divalent (cyanic) to trivalent (greenish).[11),14] Thus, for the $Li_2CoTi_3O_8$ pigment via the sol–gel method by Costa da Câmara,[12] the valence change of Co might occurred during the heat treatment of precursor samples. Whereas, for the $Li_2CoTi_3O_8$ pigment via the solid state method, which is generally suitable for the low-cost and mass production, the effect of synthetic temperature on color tone has scarcely been reported. Thus, in this study, we have synthesized $Li_2CoTi_3O_8$ pigments via solid state method at different synthetic temperatures of 500–1200 °C, and systemically studied the effect of heat-treatment temperatures on color tone, using CIE-$L^*a^*b^*$ color coordinates, hue angle h, X-ray photoelectron spectroscopy (XPS) and ultra violet–visible (UV–Vis) spectroscopy.

2. Experimental

2.1 Synthesis and phase analysis of $Li_2CoTi_3O_8$ pigment powders

Similarly to our previous study,[14] Li_2CO_3 (≥99.0%, Wako Pure Chemical Industries, Ltd.), CoO (90.0%, Wako) and TiO_2 (anatase) (99%, Kojundo Chemical Laboratory) powders were used as starting materials. To obtain stoichiometric $Li_2CoTi_3O_8$, these powders with the compositions of Li_2CO_3:CoO:TiO_2 = 1:1:3 (i.e., 20:20:60) in mol.% were used. The Li_2CO_3, CoO and TiO_2 (anatase) powders were weighed and mixed/pestled in an agate mortar for 10 min. The mixed powders in Al_2O_3 crucibles were heat-treated in air for 2 h. After the heat treatment, the synthesized $Li_2CoTi_3O_8$ powder aggregates were pestled in an agate mortar for 10 min to obtain $Li_2CoTi_3O_8$ pigment powders. In order to study the effect of synthetic temperature, total 12 samples were synthesized at different temperatures from 500 to 1200 °C. The constituent phases of the $Li_2CoTi_3O_8$ powders were analyzed by X-ray diffraction (XRD, Multiflex, Cu-Kα, 40 kV and 40 mA, Rigaku) at a scanning rate of 4 °/min. The microstructure of the $Li_2CoTi_3O_8$ powders was observed by scanning electron microscopy (SEM, SU-70, Hitachi High-Technologies).

2.2 Color characterization

The color tones of the $Li_2CoTi_3O_8$ pigments were measured with a color reader (8° illumination angle and diffuse viewing, CR-20, Konica Minolta, Japan). CIE1976-$L^*a^*b^*$ color coordinates were evaluated. The $L^*a^*b^*$ color system is close to the human eye's feeling and is superior for comparing colors. L^* represents lightness, and combinations of two values of a^* and b^* express chroma and hue. The closer the value of L^* is to 100, the lighter the white color, and the closer to 0 the darker the black color. Also, when the value of a^* is large in the positive direction, it becomes red, and when large in the negative direction, it becomes green. Also, when the value of b^* is large in the positive direction, it turns yellow and when large in the negative direction it becomes blue. In order to improve the reproducibility of the color measurement, each powder was uniaxially pressed into a pellet prior to the color measurement. For each sample, L^*, a^* and b^* values were determined as an average for 10 points.

Hue h, representing a color category, is calculated from the following equation including a^* and b^*, and it is plotted on a color circle:

$$h = \tan^{-1}\left(\frac{b^*}{a^*}\right)$$

Also, defuse reflectance spectra for the $Li_2CoTi_3O_8$ powders were measured by UV–Vis spectrometry (5° illumination angle and diffuse viewing, ARMN-735, JASCO).

2.3 Electronic state and valence analyses of cobalt ions

The electronic states and valence of cobalt ions in the $Li_2CoTi_3O_8$ powders were analyzed by XPS (JPS-9010TR, JEOL) and by electron spin resonance spectroscopy (ESR, JES-FA200, JEOL). The binding energy for XPS measurement was adjusted with carbon standard, but the absolute values may contain some systematic errors. The ESR signals were measured for ca. 60 min for each sample. The g factor and line width of the ESR signals were calibrated using a standard Mn^{2+} marker sample. More detail of the ESR setting is available elsewhere.[20]

3. Results and discussion

3.1 Crystal structure and microstructure

Figure 2 shows XRD patterns of the $Li_2CoTi_3O_8$ powders synthesized at different heat-treatment temperatures. At 500 °C, peaks of $Li_2CoTi_3O_8$, TiO_2 anatase, CoO and Li_2CO_3 were confirmed. With increasing the heat-treatment temperature, at ~650–750 °C, CoO was oxidized into Co_3O_4, and at ~750 °C, TiO_2 anatase transformed into TiO_2 rutile phase. At 850–900 °C, the sample became almost single phase $Li_2CoTi_3O_8$ with a trace amount of TiO_2 rutile. At 950–1200 °C, single phase $Li_2CoTi_3O_8$ was obtained.

Figure 3 shows SEM micrographs of the synthesized $Li_2CoTi_3O_8$ powders (observed without pelletizing). At 500 °C, the sample was composed of fine particles of ~0.1–0.2 μm. At 750 °C, particles of ~0.2–0.3 μm as well as solidified liquid phase were observed (due to the melting of Li_2CO_3 at ~726 °C). The liquid phase must accelerate the reactions among intermediate phases and the grain growth. The particle sizes of the samples heat-treated at 850, 950, 1000 and 1050 °C were ~0.5–1, ~0.5–1.5, ~1–2 and ~2 μm, respectively. These particle sizes are favorable for the pigment applications. At 1150 and 1200 °C, the heat-treated sample powder became semi-solidified, and the grain growth became severer as can be seen in SEM micrographs. The crashed samples at these temperatures had wide particle size distributions, and they

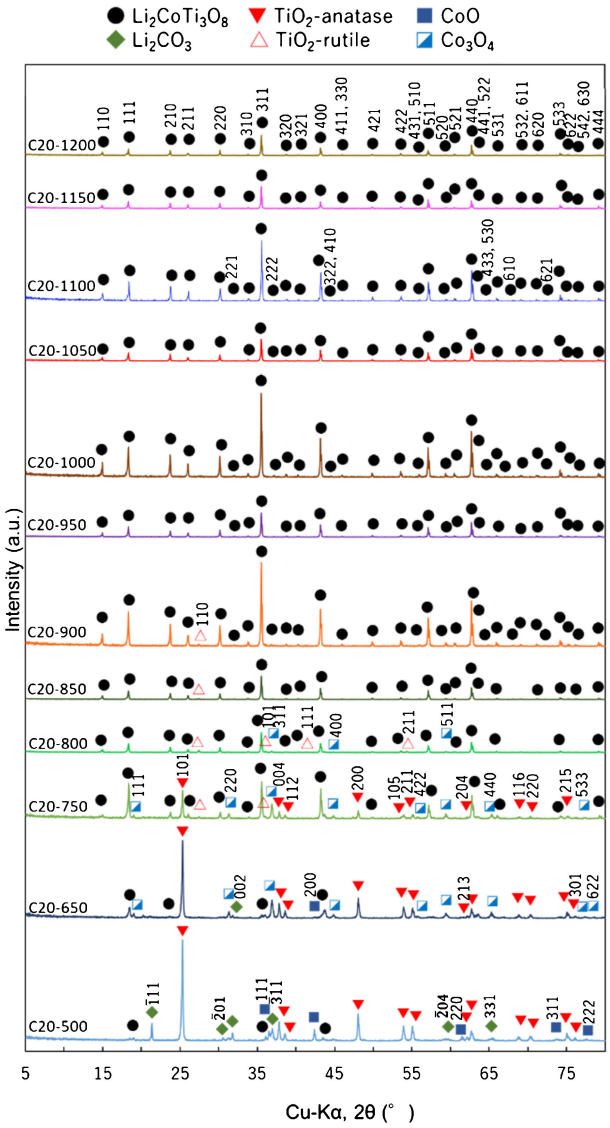

Fig. 2. XRD patterns of the $Li_2CoTi_3O_8$ powders synthesized at different heat-treatment temperatures (heat-treated in air for 2 h).

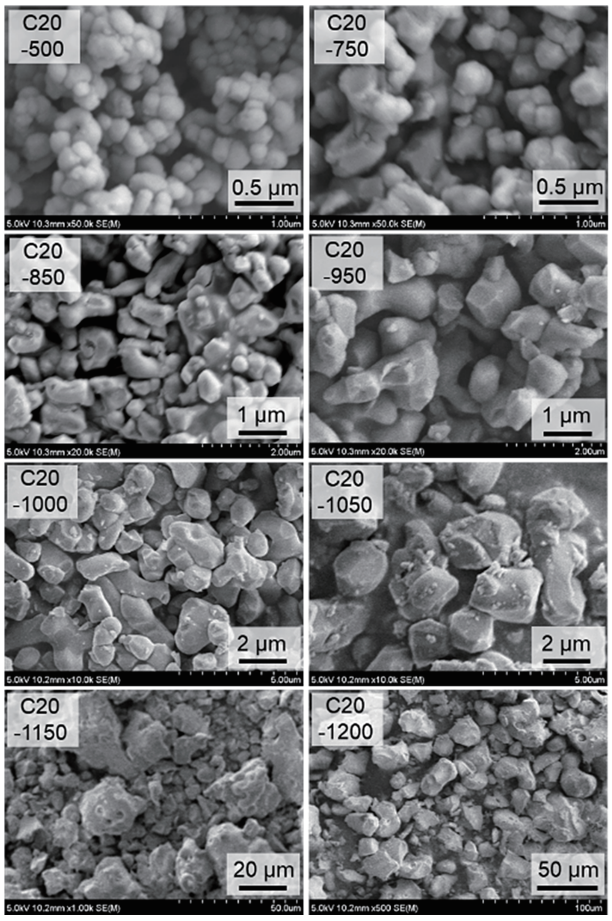

Fig. 3. SEM micrographs of the $Li_2CoTi_3O_8$ powders synthesized at different heat-treatment temperatures (heat-treated in air for 2 h).

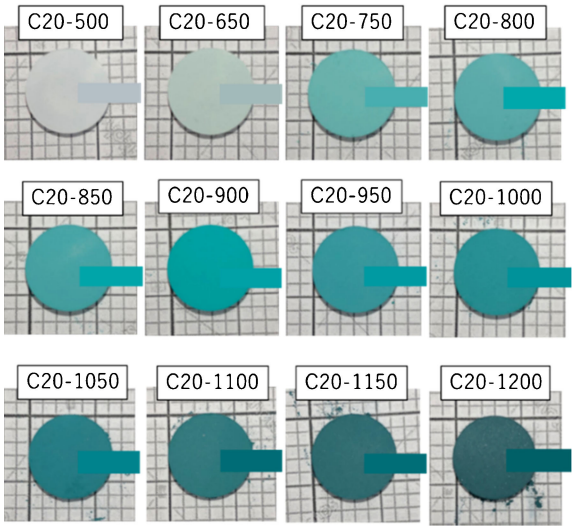

Fig. 4. Appearance of the synthesized $Li_2CoTi_3O_8$ powders with different heat-treatment temperatures (heat-treated in air for 2 h, and uniaxially pelletized). Rectangular color bars inserted in the photos are rendered by using measured L^*, a^* and b^* values.

are not suitable for the pigment powders without a further milling treatment.

3.2 Sample appearance and color characterization

Figure 4 demonstrates appearances of the synthesized $Li_2CoTi_3O_8$ powders with different heat-treated temperatures. Rectangular color bars inserted in the photos are rendered by using measured L^*, a^* and b^* values with Irodashi-Meijin-Pro software ver. 2.00. The C20-500 sample was whitish and almost the same color as the powder mixture. C20-650 was still whitish but with very weak cyan-tone. C20-750 started to show pale cyanic tone. From C20-800 to C20-1000 samples, cyanic-tone gradually became deeper with increasing the heat-treatment temperatures. From C20-1050 to C20-1200 samples, the cyanic tone became much deeper.

In order to quantitatively compare the sample colors, CIE1976-$L^*a^*b^*$ color coordinates were evaluated with a color reader as shown in **Fig. 5**. With increasing the heat-treatment temperatures, brightness value, L^*, monotonically decreased due to (1) the disappearance of colorless

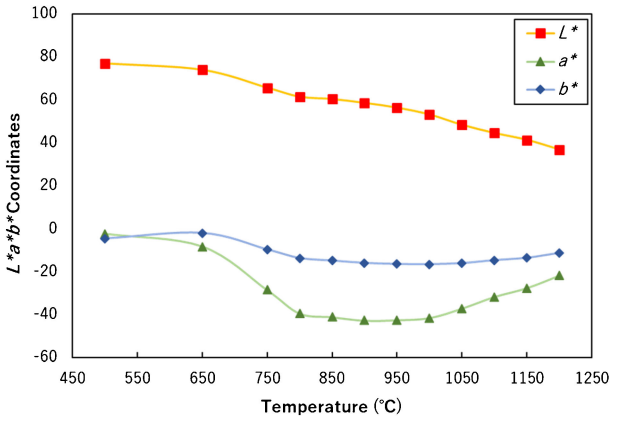

Fig. 5. CIE-$L^*a^*b^*$ color coordinates of the synthesized $Li_2CoTi_3O_8$ powders with different heat-treatment temperatures (heat-treated in air for 2 h, and uniaxially pelletized as shown in Fig. 4).

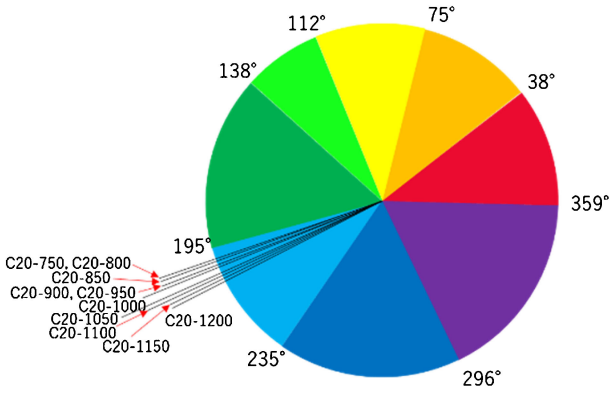

Fig. 6. Hue angle h of the synthesized $Li_2CoTi_3O_8$ powders with different heat-treatment temperatures (heat-treated in air for 2 h, and uniaxially pelletized as shown in Fig. 2), displayed on a 2-D simplified $L^*a^*b^*$ color space diagram cut in the horizontal direction.

TiO_2 phases (see Fig. 2) and (2) the increase of particle size (see Fig. 3). For the samples C20-500 and C20-650, the a^* and b^* values were close to zero (and $L^* > 70$), which indicate the sample colors were whitish as observed in Fig. 4. For C20-750 and C20-800, the a^* value obviously became large in minus direction (i.e., became greenish) and the b^* value slightly became minus (i.e., became pale blue). Since the L^* values of these samples were still around 60–65, the C20-750 showed light cyanic tone and the C20-800 become slightly deeper but still pale cyanic. For C20-800 to C20-1000, a^* and b^* values were almost unchanged but L^* gradually decreased, which was in good agreement with the appearance shown in Fig. 4. From C20-1050 to C20-1200, a^* was still minus but $|a^*|$ became smaller (i.e. less greenish) with increasing the heat-treatment temperatures. For these samples, change of $|b^*|$ was not so prominent as $|a^*|$. Hence, from C20-1050 to C20-1200, green component became apparently weaker, while blue component became just slightly weaker. With considering the decrement of brightness, L^*, in total, from C20-1050 to C20-1200, deeper cyanic color with higher blue tone was observed for these samples.

Figure 6 shows hue angle h of the synthesized $Li_2CoTi_3O_8$ powders with different heat-treatment temperatures displayed on a 2-D simplified $L^*a^*b^*$ color space diagram cut in the horizontal direction. Note that the C20-500 and 650 samples were not plotted on this figure due to their insufficient coloring. All the samples from C20-750 to C20-1200 located in the cyan color zone ($h \sim 195$–235°). In our previous report,[14] we have demonstrated that $Li_2CoTi_3O_8$ pigments with CoO-lean or stoichiometric CoO compositions displayed cyan color while those with CoO-rich composition had green color. This cyan-green dichroism of the $Li_2CoTi_3O_8$ pigment can be attributable to the valence change of the Co ions from divalent (cyanic) to trivalent (greenish). In the current study, on the other hand, such a dichroism was not observed, which suggests that the effect of heat-treatment temperatures on the valence of Co ions was not so prominent up to 1200 °C; a major part

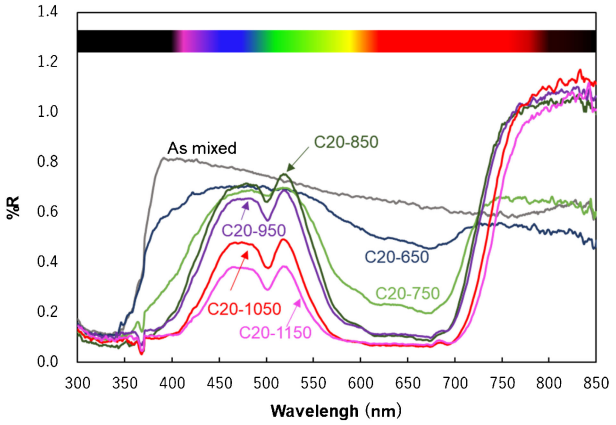

Fig. 7. UV–Vis defuse reflectance spectra of the synthesized $Li_2CoTi_3O_8$ powders with different heat-treatment temperatures. Prior to the UV–Vis measurements, the sample pellets in Fig. 4 were further cold-isostatically-pressed at 200 MPa just to keep the compact shape and to improve the handling.

of Co ion should remain divalent (cyanic). The valence of Co ions will be discussed in more detail in the latter part of this paper.

3.3 UV–Vis analyses

Figure 7 shows UV–Vis defuse reflectance spectra of the synthesized $Li_2CoTi_3O_8$ powders with different heat-treatment temperatures. An as-mixed sample (without heating) and six heat-treated samples (C20-650, 750, 850, 950, 1050 and 1150) were evaluated. The as-mixed and C20-650 samples homogeneously reflected the incident light for whole the visible wavelength, which resulted in whitish appearances as shown in Fig. 4.

The C20-750 sample absorbed visible light with the wavelength of mainly about 570–680 nm, corresponding to greenish yellow and red regions. The C20-750 absorbed the wavelength also of ~490 nm, but it was very weak. The visible light absorptions of ~490 nm (weak) and ~570–680 nm (strong) are attributable to the absorption bands

of Co^{2+} with *tetrahedral* 4-coordination, namely around 480–490, 550–570, 590–610 and 620–660 nm.[21)–23)] Since the absorption bands at 550–570, 590–610 and 620–660 nm are particularly strong, they absorb the light from greenish yellow to red. As shown in XRD analysis (Fig. 2), in the C20-750, there existed unreacted TiO_2 anatase (and some other oxides), which resulted in whole visible-length reflections (i.e whitish appearance). Therefore, the C20-750 represented pale cyanic (i.e. weak greenish blue) tone.

For the samples heat-treated at ≥850 °C, the reflectance became smaller with increasing the heat-treatment temperatures. This tendency was in good agreement with the sample appearances as shown in Fig. 4, where the sample color became darker with increasing the heat-treatment temperatures. The C20-850 and 950 samples had deeper absorption band of 560–700 nm than the C20-750. Also, the small absorption at ~500 nm became apparent for these samples. These absorption bands are attributable to the absorption bands of Co^{2+} with tetrahedral coordination, similarly to C20-750. Since the C20-850 and 950 samples contained less unreacted oxide phases (i.e., less whitish component), the sample colors became close to the intrinsic color of cyanic $Li_2CoTi_3O_8$.

The C20-1050 and 1150 samples had somewhat weaker reflections at around 400–550 nm (Fig. 7) and thus they had somewhat deeper cyanic tone (Fig. 4), because the absorption bands of Co^{2+} with *octahedral* 6-coordination locate between violet and green region.[22)] These results indicated that at higher heat-treatment temperatures, Co^{2+} ions occupy not only the tetrahedral site but also the octahedral site, which is in good agreement with the previous report by Reeves et al. on the order–disorder transition in $Li_2CoTi_3O_8$.[16)] We have also confirmed the order–disorder transition by using our high-temperature XRD measurement (see Fig. S1).

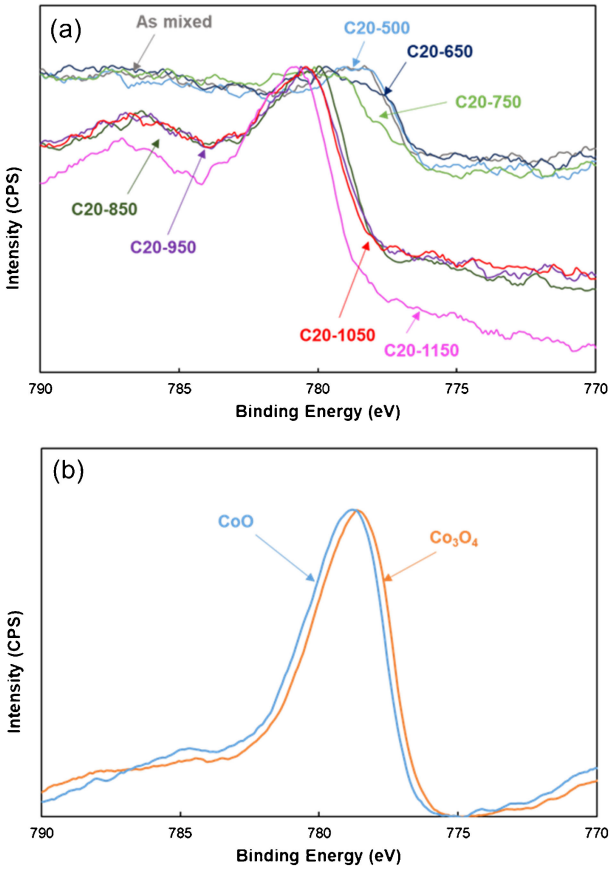

Fig. 8. Co 2p3/2 X-ray photoelectron spectra for (a) the synthesized $Li_2CoTi_3O_8$ powders with different heat-treatment temperatures, and (b) commercial CoO (a starting material of this study) and Co_3O_4 powders as references. The binding energy (horizontal axis) was adjusted with carbon standard and the intensities (vertical axis) was normalized with the peak-top intensities. Note that the background was subtracted for CoO and Co_3O_4 in (b).

3.4 Electronic state of Co ions: XPS analysis

In order to investigate the origin of the color difference with changing the heat-treatment temperatures, the electronic state of Co ions was examined by XPS measurement. **Figure 8**(a) shows Co 2p3/2 XPS analysis for the synthesized $Li_2CoTi_3O_8$ powders with different heat-treatment temperatures. Total 8 samples, *viz*., as-mixed, C20-500, 650, 750, 850, 950, 1050 and 1150, were analyzed. As can be seen from Fig. 8(a), peak shapes were roughly categorized into two groups, i.e., (i) as mixed, C20-500 and C20-650, and (ii) C20-850, C20-950, C20-1050 and C20-1150. The spectrum for C20-750 was in-between these two groups. For the group (i), as-mixed and heat-treated at lower temperatures, the main peak located at ~778 eV. Since the Co-containing phases in the group (i) were mainly CoO (and trace Co_3O_4) as shown in Fig. 2, the main peak at ~778 eV is mainly attributable to CoO (and Co_3O_4), which is confirmed by the XPS measurements for commercial CoO and Co_3O_4 powders as references [Fig. 8(b)]. The low binding energy (~778 eV) for CoO and Co_3O_4 containing samples (as-mixed, C20-500, C20-650) might be explained by the non-stoichiometric nature of the starting CoO powder. For the group (ii), heat-treated at higher temperatures, the main peak located at ~781 eV. As the Co-containing phase in the group (ii) was $Li_2CoTi_3O_8$ (Fig. 2), the main peak at ~781 eV is attributable to $Li_2CoTi_3O_8$. From these results, binding energy for Co ions became larger when they were incorporated into the $Li_2CoTi_3O_8$ spinel structure.

3.5 Valence of Co ions: ESR analysis

In Section 3.4, we have focused on the binding energy of Co ions using XPS analysis. For the Co-based blue pigments, the valence of the Co ions also plays important roles. In our previous paper,[14)] we have concluded that the valence of Co ions in the stoichiometric $Li_2CoTi_3O_8$ pigment are mainly Co^{2+} (divalent), and that in the CoO-rich $Li_2CoTi_3O_8$ pigment are the mixture of Co^{2+} (divalent) and Co^{3+} (trivalent), which are suggested by the XPS analysis. In this study, since the stoichiometric composition (i.e. C20) was studied, the valence of Co ions will be mainly Co^{2+}.

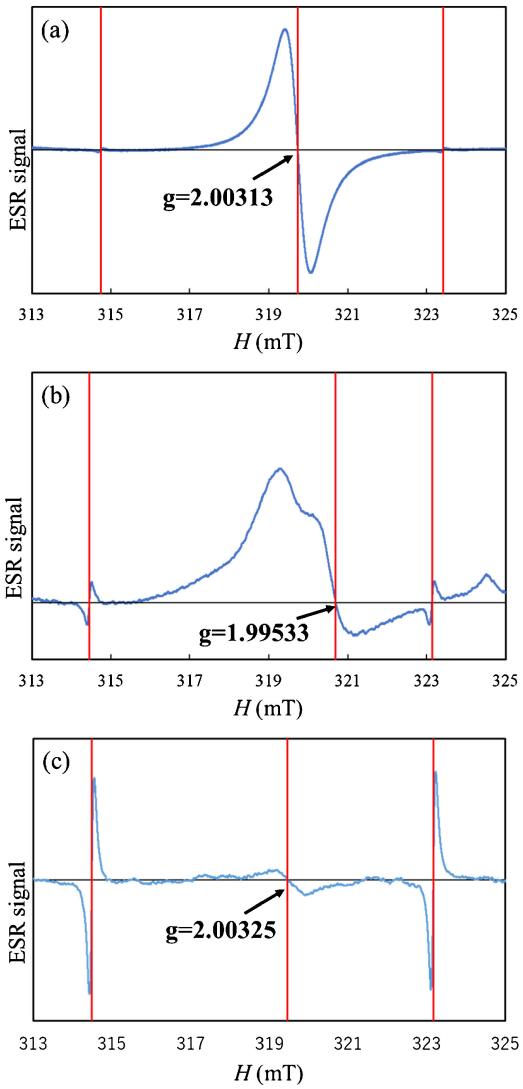

Fig. 9. ESR spectra of (a) CoO starting powder, (b) C20-650 and (c) C20-1100.

To verify the valence of Co ions in this study, ESR analysis was also carried out (**Fig. 9**). The *g* factor, reflecting the environment of electron spins, was calibrated using a standard Mn^{2+} marker sample (left and right-side vertical red lines). Figure 9(a) shows an ESR spectrum for the CoO starting powder. In this sample, the valence of Co ions was mainly Co^{2+}. The ESR signal at 319.7 mT was very large and the *g* value for this sample was 2.00313. Next, Fig. 9(b) shows an ESR spectrum for the C20-650 sample. As can be seen from the spectrum shape, it is considered that two peaks are overlapped. The large peak around 319 mT is attributed to the unreacted CoO (as discussed in XRD analysis) and another peak at 320 mT is then attributable to a certain defect around the Co ions, which implies the incompleteness of the solid state reactions at 650 °C. Due to the existence of this second signal, the *g* value for this sample was 1.99533. Figure 9(c) shows an ESR spectrum for the C20-1100 sample. Although the signal intensity was small as compared with Fig. 9(a), the *g* value for this sample was 2.00325, which indicates the existence of Co^{2+}. The weakness of the ESR signal for the C20-1100 sample can be explained as follows. As reported by Reeves et al.,[16] there is an order–disorder transition for $Li_2CoTi_3O_8$. From ambient to middle temperatures, Co^{2+} ions occupy the tetrahedral site (4-coordinations, high-spin) in the ordered spinel structure with the space group of $P4_332$. However, at higher temperatures, some Co^{2+} ions also occupy the octahedral site (6-coordinations, high-spin or low-spin) in the disordered spinel structure with the space group of $Fd\bar{3}m$. In the C20-1100 sample, although it was not quenched from a high temperature, Co^{2+} ions in the octahedral site still remained even at the ambient temperature. That is why Co^{2+} ions with low-spin state (6-coordinations) existed in the sample, and they decreased electron spin intensities.

4. Conclusions

In this study, we have synthesized $Li_2CoTi_3O_8$ pigments via solid state method at different synthetic temperatures of 500–1200 °C, and studied the effect of heat-treatment temperatures. In conclusions:

(1) At 500 °C, the sample consisted of $Li_2CoTi_3O_8$, TiO_2 anatase, CoO and Li_2CO_3. At ~650–750 °C, CoO was oxidized into Co_3O_4, and at ~750 °C, TiO_2 anatase transformed into TiO_2 rutile. At 850–900 °C, almost single phase $Li_2CoTi_3O_8$ with a trace amount of TiO_2 rutile was obtained. At 950–1200 °C, single phase $Li_2CoTi_3O_8$ was obtained.

(2) C20-500 sample was whitish, and C20-650 was still whitish but with very weak cyan-tone. C20-750 started to show pale cyanic tone. From C20-800 to C20-1000 samples, cyanic-tone gradually became deeper with increasing the heat-treatment temperatures. From C20-1050 to C20-1200 samples, the cyanic tone became much deeper.

(3) All the samples from C20-750 to C20-1200 located in the cyan color zone ($h \sim 195$–$235°$). In this work, the cyan-green dichroism was not observed, which suggests that the effect of heat-treatment temperatures on the valence state of Co ions was not so prominent up to 1200 °C; a major part of Co ion should remain divalent (cyanic). From UV–Vis defuse reflectance spectra, the color change was explained by the visible light absorptions of Co^{2+} with *tetrahedral* 4-coordination and Co^{2+} with *octahedral* 6-coordination, which were also verified by XPS and ESR analyses.

Acknowledgment A part of this work was supported by JSPS-KAKENHI Grant Number JP16H04212 for Basic Research: Category B, and Joint Research Project of JWRI, Osaka University. We thank the Open Facility Network Office, Research Facility Center for Science and Technology, University of Tsukuba, for the XPS and UV–Vis measurements. We also thank Dr. Momma and Dr. Izumi for offering a crystal drawing free software VESTA Ver. 3.[24]

References

1) M. Bouchard and A. Gambardella, *J. Raman Spectrosc.*, 41, 1477–1485 (2010).

2) M. Yoneda, I. Gotoh, M. Nakanishi, T. Fujii and T. Nomura, *Powder Technol.*, 323, 574–580 (2018).
3) A. A. Ali, E. El Fadaly and I. S. Ahmed, *Dyes Pigments*, 158, 451–462 (2018).
4) M. Yoneda, K. Gotoh, M. Nakanishi, T. Fujii, Y. Konishi and T. Nomura, *J. Am. Ceram. Soc.*, 102, 3468–3476 (2019).
5) S. Jose and M. L. Reddy, *Dyes Pigments*, 98, 540–546 (2013).
6) J. Li, E. A. Medina, J. K. Stalick, A. W. Sleight and M. A. Subramanian, *Prog. Solid State Ch.*, 44, 107–122 (2016).
7) A. Fernández-Osorio, M. P. Jiménez-Segura, A. Vázquez-Olmos and R. Sato-Berru, *Ceram. Int.*, 37, 1465–1471 (2011).
8) Wendusu, T. Honda, T. Masui and N. Imanaka, *Chem. Lett.*, 42, 1562–1564 (2013) (*no initial for Wendusu).
9) J. Li and M. A. Subramanian, *J. Solid State Chem.*, 272, 9–20 (2019).
10) J. W. Nuss, US Patent No. 4075029 (1978).
11) A. Kimura, Y. Ikuta and F. Suzuki, *Shikizai*, 69, 810–818 (1996) [in Japanese].
12) M. S. C. da Camara, L. A. Pimentel, E. Longo, L. de Nobrega Azevedo and D. M. de Araujo Melo, *Bol. Soc. Esp. Ceram. V.*, 55, 71–78 (2016) [in Spanish].
13) M. S. C. da Camara, Ph. D. thesis, Federal University of São Carlos, Brazil (2004).
14) S. Kimura and Y. Suzuki, *Ceram. Int.*, 45, 12602–12607 (2019).
15) H. Kawai, M. Tabuchi, M. Nagata, H. Tukamoto and A. R. West, *J. Mater. Chem.*, 8, 1273–1280 (1998).
16) N. Reeves, D. Pasero and A. R. West, *J. Solid State Chem.*, 180, 1894–1901 (2007).
17) W. Chen, R. Du, W. Ren, H. Liang, B. Xu, J. Shu and Z. Wang, *Ceram. Int.*, 40, 13757–13761 (2014).
18) L. Wang, Q. Z. Xiao, Z. H. Li, G. T. Lei, L. J. Wu, P. Zhang and J. Mao, *Electrochim. Acta*, 77, 77–82 (2012).
19) J. Wang, H. Zhao, Y. Shen, Z. Du, X. Chen and Q. Xia, *ChemPlusChem*, 78, 1530–1535 (2013).
20) Y. Sakurai, D. Matsumoto and K. Marumoto, *Appl. Magn. Reson.*, 49, 767–782 (2018).
21) O. Schmitz-DuMont, H. Brokopf and K. Burkhardt, *Z. Anorg. Allg. Chem.*, 295, 7–35 (1958) [in German].
22) A. Ohtsuka, *J. Ceram. Assoc. Jpn.*, 73, 196–206 (1965) [in Japanese].
23) M. N. Taran, M. Koch-Muller and A. Feenstra, *Am. Mineral.*, 94, 1647–1652 (2009).
24) K. Momma and F. Izumi, *J. Appl. Crystallogr.*, 44, 1272–1276 (2011).